JTTEE5 12:393-402

Deposition of Nanoparticle Suspensions by Aerosol Flame Spraying: Model of the Spray and Impact Processes

T. Poirier, A. Vardelle, M.F. Elchinger, M. Vardelle, A. Grimaud, and H. Vesteghem

(Submitted 1 February 2002; in revised form 16 April 2002)

Aerosol flame spraying (AFS) combines the atomization of a colloidal suspension with the lateral injection of the aerosol in a flame. The aerosol droplets are partially dried when crossing the flame and then deposited as a coating onto a substrate. Afterwards, the coating is consolidated by heat treatment without extensive grain growth. In this paper a model of the trajectories, acceleration and vaporization of the droplets is used to predict the impact conditions of the in-flight dried droplets, as well as their size and water content when they impinge onto the substrate. From these calculations and the hydrodynamic properties (viscosity, surface tension, contact angle) of the suspensions, the morphology and size of the lamellae deposited on the substrate are determined by using classic impact models. In spite of the complexity of the mixing of the suspension spray with the flame and the diversity of the thermal histories of the droplets, the observation of the latter after impact shows that the results of the model are quite consistent with measurements. The relationship between droplet impact parameters and coating formation is discussed.

Keywords colloids, flame spraying, impact, modeling, suspension, zirconia

1. Introduction

The Aerosol flame spraying (AFS),[1-3] is a sol-based deposition process. This technique has features in common with a spray drying method as it combines the pulverization of the sol solution with injection and heating in an oxyacetylene flame (Fig. 1). The aim of such a technique is to partially dry the aerosol droplets when they cross the flame and project them onto a substrate where they form a coating. The AFS technique can be used to produce nanostructured and polycrystalline coatings from a nanoscale powder as the material is exposed to high temperatures only during a short time. The coating is further consolidated by a thermal treatment without extensive grain growth.[4] For zirconia colloidal suspensions with 60-nm original grain size, the densification begins below 1000 °C and is complete at 1100 °C.[4] Recent works have shown that for zirconia suspensions with 30-nm grain size, the densification is complete below 800 °C.[5]

In AFS, the deposition mechanisms of the droplets onto the substrate depend on (1) the hydrodynamic properties (viscosity, surface tension contact angle) of the sol as a function of its solid content, (2) the original droplet diameter, (3) the thermokinematic history of the droplets before they impinge on the substrate, and (4) the roughness, chemistry and temperature of the substrate surface. The optimization of the process to produce nanostructured coatings with desired properties requires a broad understanding of the phenomena, which occur during the residence of the droplets in the flame and after their impact onto the substrate. The present work addresses the use (1) of a 2D numerical model for the prediction of the diameter, velocity, and drying level of the droplets at impact and (2) of an analytical model[6-13] for the estimation of the effect of the droplet zirconia content on the size and morphology of the lamellae formed after impact on the substrate.

T. Poirier, Universidad Simon Bolivar, Caracas, Venezuela; **A. Vardelle, M.F. Elchinger, M. Vardelle,** and **A. Grimaud,** University of Limoges, Limoges, France; and **H. Vesteghem,** Ecole Nationale Supérieure de Céramique Industrielle, Limoges, France. Contact e-mail: tpoirier@usb.ve.

2. Experimental

In the present work, the suspensions were prepared by two-step hydrolysis of a zirconium oxyacetate precursor in an auto-

Nomenclature

Leidenfrost point	breakup temperature of evaporable liquid droplets on a hot substrate
MMD	mass mean diameter
D	diameter
A	surface
M	mass flow
m	a dimensional constant in Kim-Marshall equation
ρ	density
σ	surface tension
μ	viscosity
V	velocity
ξ	flattening rate
θ	contact angle
k	thermal conductivity
Re	Reynolds number
We	Weber number
Oh	Ohnesorge number
K	Sommerfeld number
Bi	Biot number

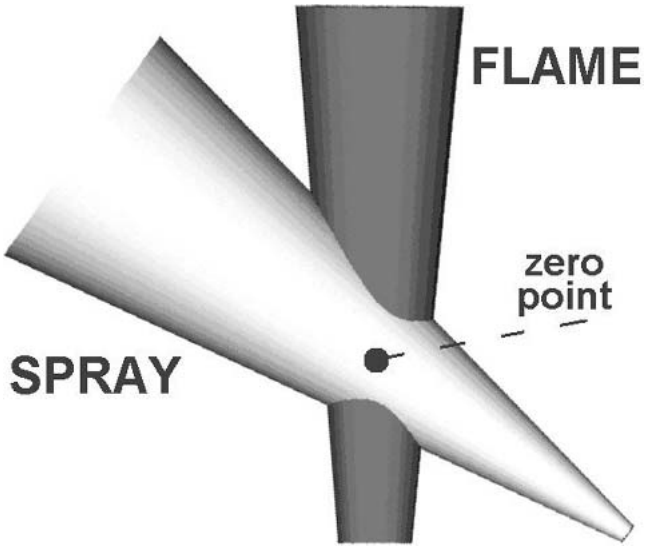

Fig. 1 Injection of the zirconia colloidal suspension into the flame: theoretical crossing of the suspension spray and flame.

clave at 270 °C.[2,4] The diameter of the colloidal particles was about 60 nm and the solid content of the sol particles was 18.5 wt.%. The sol droplets will be partially dried in the flame during the deposition process. Therefore, the heating will cause a concentration of the solid content of the droplets. The knowledge of the hydrodynamic properties of the sol droplets as a function of their solid content is a requirement for the modeling of their behavior in the flame. Thus, suspensions with solid concentrations ranging between 18.5 and 40 wt.% were prepared by slowly drying the suspensions on a sand bath maintained at 100 °C. The density, viscosity, surface tension and angle of contact of these various suspensions were characterized. The viscosity was determined with a Brookfield viscosimetric cell (PVS Rheometer, Brookfield, Middleboro, MA) at a temperature of 30 °C and a hermetic plastic cap to avoid water evaporation. The surface tension (inferred from the geometry of the droplet) is measured by the pendant drop technique using a CCD camera.[14] A similar method was used to measure the contact angle on an AISI 316L polished (Ra = 0.3 μm) substrate washed with ethanol.

A SATA Minijet pneumatic gun (Sata Gmbh, Kornwestheim, Germany) was used to pulverize the zirconia suspension and form an aerosol. The main operating parameters of this gun were the following: air pressure = 2 or 4 bars, airflow rate = 33 or 66 slm, and liquid flow rate = 0.006 slm. The air velocity at the tip of the spray gun exit, measured using a Pitot tube, was 280 m/s at 2 bars and 310 m/s at 4 bars. According to Masters,[15] the mass mean diameter (MMD) of the droplets atomized by an aerographic gun follows the Kim-Marshall equation:

$$\mathrm{MMD} = \left[\frac{249\sigma^{0.41}\mu^{0.32}}{(V_a^2 \cdot \rho_a)^{0.57} \cdot A^{0.36}\rho^{0.16}}\right] + 1260\left[\left(\frac{\mu_l}{\rho_l\sigma}\right)^{0.17} \cdot \left(\frac{1}{V_a^{0.54}}\right) \cdot \left(\frac{M_a}{M_l}\right)^{m}\right] \quad \text{(Eq 1)}$$

where MMD is expressed in μm; ρ_a is the density of air (lb/ft^3); A is the surface of the air ring around the liquid tip of the nozzle (in^2); M_l is the liquid mass flow (lb/min); M_a is the air mass flow (lb/min) and m, a constant equal to −1 if $(M_a/M_l) < 3$, otherwise m is equal to −0.5; and ρ_l, σ, μ_l are the density (lb/ft^3), surface tension (dynes/cm), and viscosity of the liquid (cP), respectively.

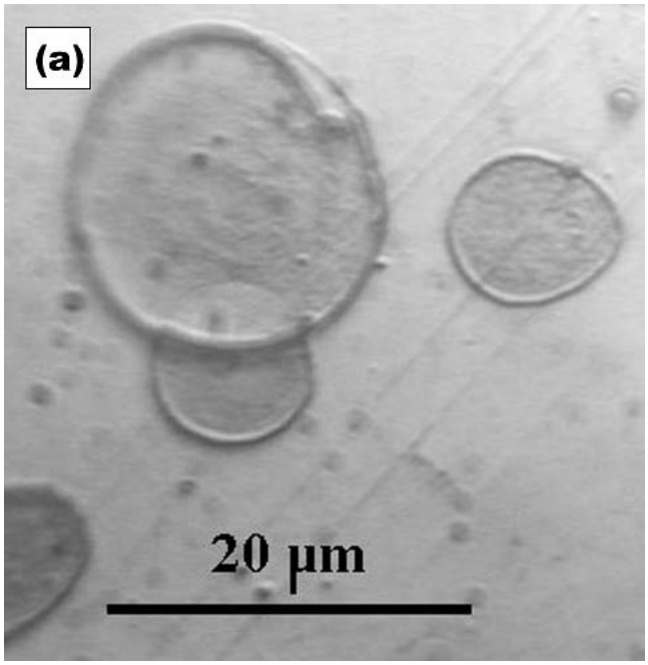

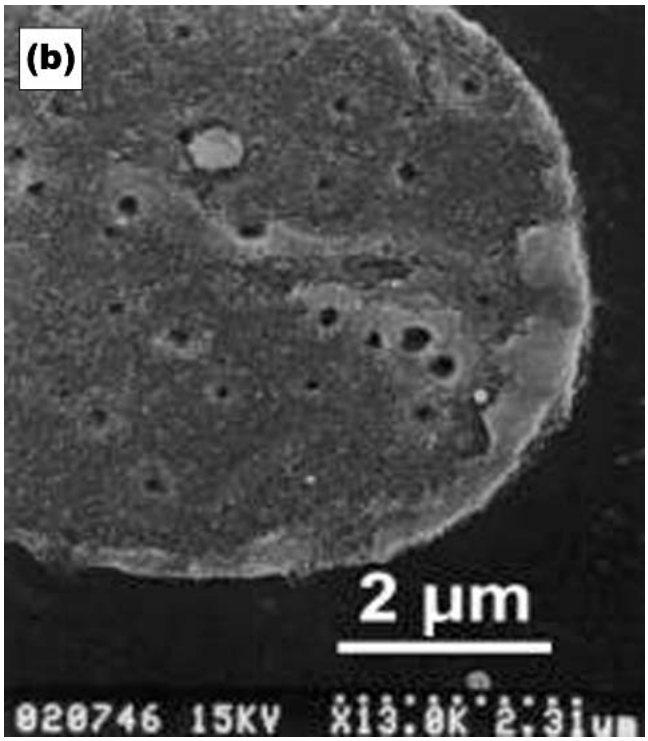

Fig. 2 **(a)** Optical microscopy of the droplets after impact on the substrate (solid concentration: 5 wt.%, substrate temperature: 25 ºC), **(b)** SEM picture of a splat (same conditions)

Under the conditions of the current study, the mass mean diameter was of the order of 12-18 μm, and the droplet diameter

distribution ranged between 0 and 60 μm depending on the air pressure used for the spray gun:

A Castolin-Eutectic Castodyn DS8000 flame torch (Castolin Eutectic Group, Kriftel, Germany) was used to heat the sprayed droplets. The centerline of the oxyacetylene flame (C_2H_2: 16.3 slm, O_2: 14 slm) made an angle of 55° with the centerline of the aerographic gun as shown in Fig. 1. This angle value is selected from previous experiments[16] where better heating of droplets was observed. The flame axis crossed the aerosol jet axis at a distance of 28 mm from the torch exit and 46 mm from the aerographic gun. This intersection point was considered as the zero point of the coordinate system used in the calculations of the in-flight droplet behavior.

The temperature field of the flame-aerosol spray system was determined using an *S* thermocouple. The temperature of the latter was corrected to take into account the radiation exchange between the thermocouple and surroundings and the conduction through the leads.[17] The velocity field was measured by seeding the flame with submicronic alumina particles and measuring their velocity using a laser Doppler velocimeter. Temperature and velocity measurements were made along a two-dimensional grid with 5 mm increments in both directions. The grid was perpendicular to the aerographic gun at 45, 80, and 120 mm from the aerographic gun exit. The distribution of the aerosol droplets was observed by focusing a laser beam through the droplet/gas jet and using a photoelectric detector to measure the bursts of light scattered when the droplets crossed the laser beam. A uniform laser sheet was generated at a right angle to the jet flow by employing a mirror oscillating at 2400 Hz.

The sprayed droplets were collected, over short times, at a distance of 100 mm from the aerographic gun (54 mm from the zero point) onto polished AISI 316L substrates maintained at room temperature or heated up to 350 °C. The surface of the substrates was observed with an Olympus PME optical microscope and a Hitachi SC2500 (Hitachi High-Technologies Corp., Tokyo, Japan) scanning electron microscope (SEM). The former technique allows the observation of large areas (a few square millimeters), but its lack of resolution limits the study to the determination of the diameters of the larger splats (Fig. 2a), while SEM enables the observation of the morphology of the splats and solidified material resulting from the impact of the droplets onto the substrate (Fig. 2b). Microscopy also permitted observation of the shape and morphology of the "objects" collected on the substrate at a given sol concentration.

Coatings were made using a rotating sample-holder with a controlled substrate-preheating rate. The coatings were studied by SEM and their thickness measured by optical microscopy.[3]

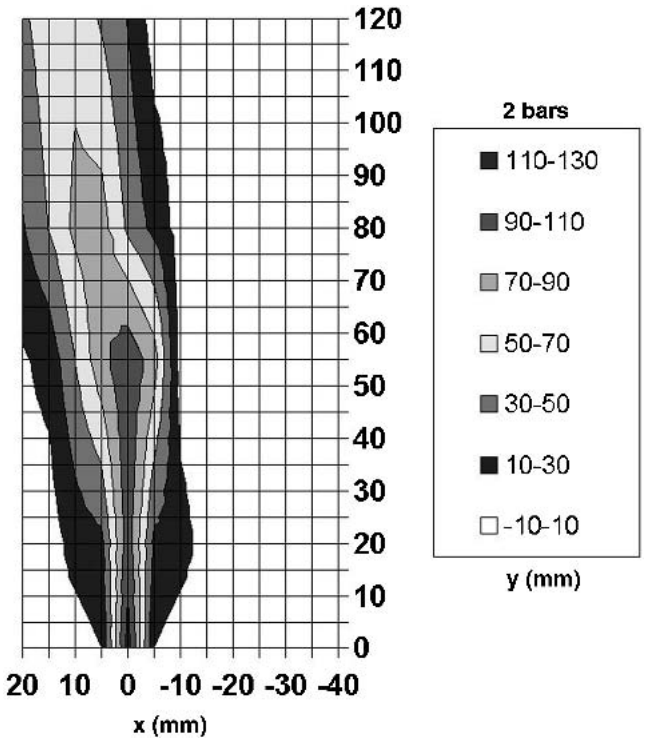

Fig. 3 Velocity contours of the flame-aerosol spray jet in the horizontal plane. Aerographic gun air pressure: 2 bars

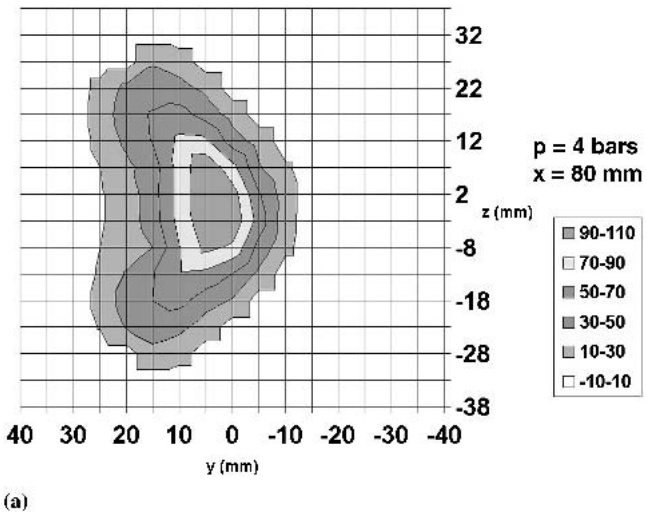

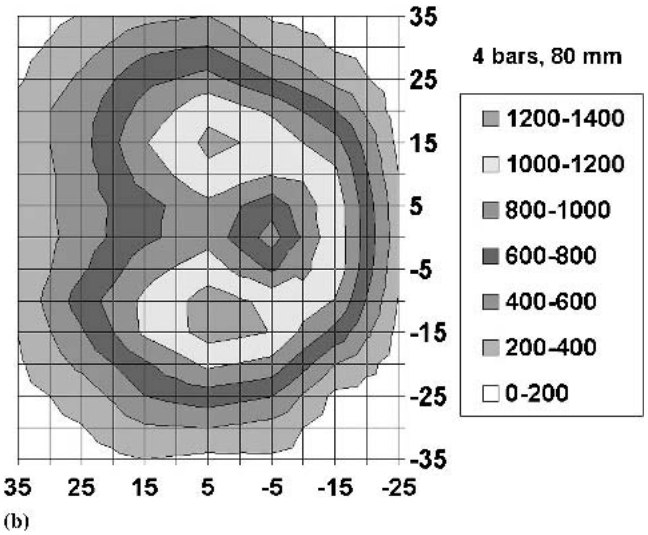

Fig. 4 **(a)** Velocity contours in a plane orthogonal to the gun axis at 80 mm from the exit of the aerographic gun. **(b)** Temperature contours at the same distance. Aerographic gun air pressure: 4 bars

3. Results

3.1 Hydrodynamic Properties of the Sol

A significant change in the behavior of the dried suspension was observed at about 32 wt.% solid concentration; an appreciable increase in viscosity was associated with a change in wettability resulting from the formation of small crusts at the surface of the drying liquid. However, these crusts did not affect the drying velocity as long as the solid concentration was lower than 75 wt.%. The observed constant rate in drying velocity backed up the assumption that the suspension droplets acted as pure water droplets although crusts might appear during the drying process.

3.2 Crossing of the Aerosol Spray With the Oxyacetylene Flame

Figure 3 shows the velocity contours of the flame-aerosol spray system in the horizontal plane and Fig. 4(a) and 4(b), the velocity and temperature contours, respectively, in a plane perpendicular to the gun centerline at a distance of 80 mm from the aerographic gun exit.

The analysis of the velocity and temperature fields of the flame-aerosol spray system showed that

- The aerosol spray jet was deflected slightly by the flame as the latter had a momentum less than that of the aerosol jet. The deflection angle was equal to 15° and 10° when the aerographic gun air pressure was 2 and 4 bars, respectively.
- The very center of the flame-aerosol spray jet system was colder than the periphery since the oxyacetylene flame had a corona shape.
- The distribution of the aerosol droplets in the spray exhibited roughly a Gaussian shape. Therefore, only a minor part of the droplets traveled in zones where the temperatures were higher than 1000 °C.
- The gas temperature and velocity contours exhibited a certain degree of symmetry round the centerline of the aerosol spray jet when taking into account the deflection of the jet by the flame. This last observation allowed the use of two-dimensional software to calculate the in-flight behavior of the droplets with certain credibility.

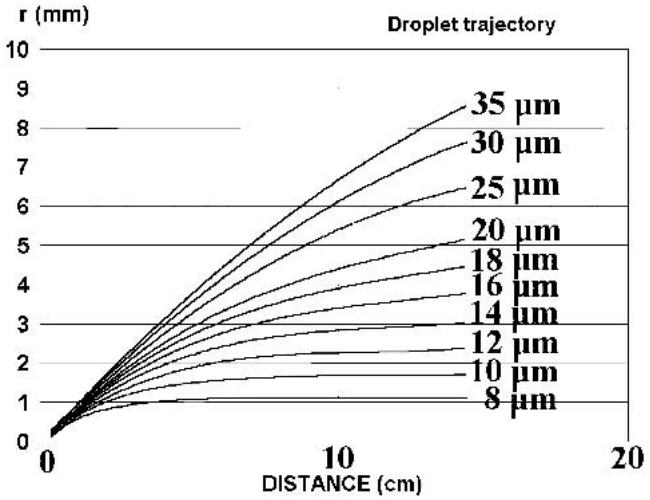

Fig. 5 Predicted radial deflection of droplets (from the zero point versus original diameter). Gun air pressure: 4 bars

3.3 Modeling of Droplet Behavior in Flight

The numerical simulations were made using a 2D computational code developed at SPCTS Laboratory (internal use), University of Limoges, for the modeling of the heating and acceleration of particles or droplets injected in a hot gas.[18] The experimental fields of gas velocity, temperature, and composition were used as input data.

The governing equations modeled the motion of the droplets and their heating and evaporation. The droplets were assumed to be spherical during the whole treatment. The equation of droplet motion was established from a force balance and accounted for the viscous drag force, pressure gradient term, and gravitational force. The temperature and evaporation rate of the droplets were inferred from an energy balance taking into account convective transfer and radiation emitted by the droplet as well as the mass

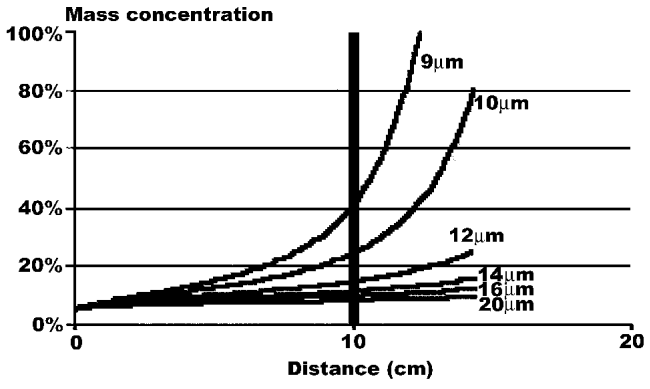

(a)

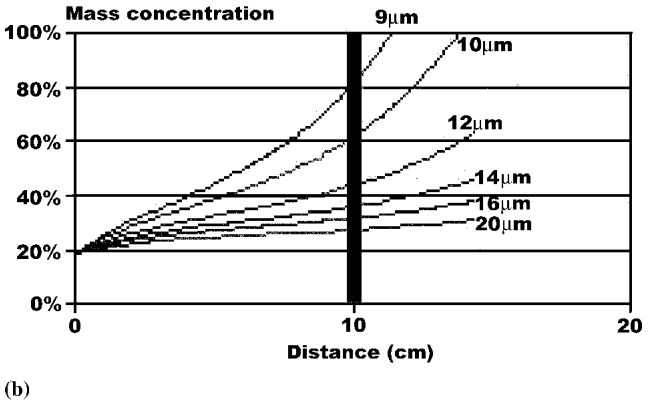

(b)

Fig. 6 **(a)** Zirconia content in droplets vs distance from the zero point for various droplet diameters for 5 wt.% zirconia concentration in original droplet. **(b)** Zirconia content in droplets vs distance from the zero point for various droplet diameters for 18.5 wt.% zirconia concentration in original droplet

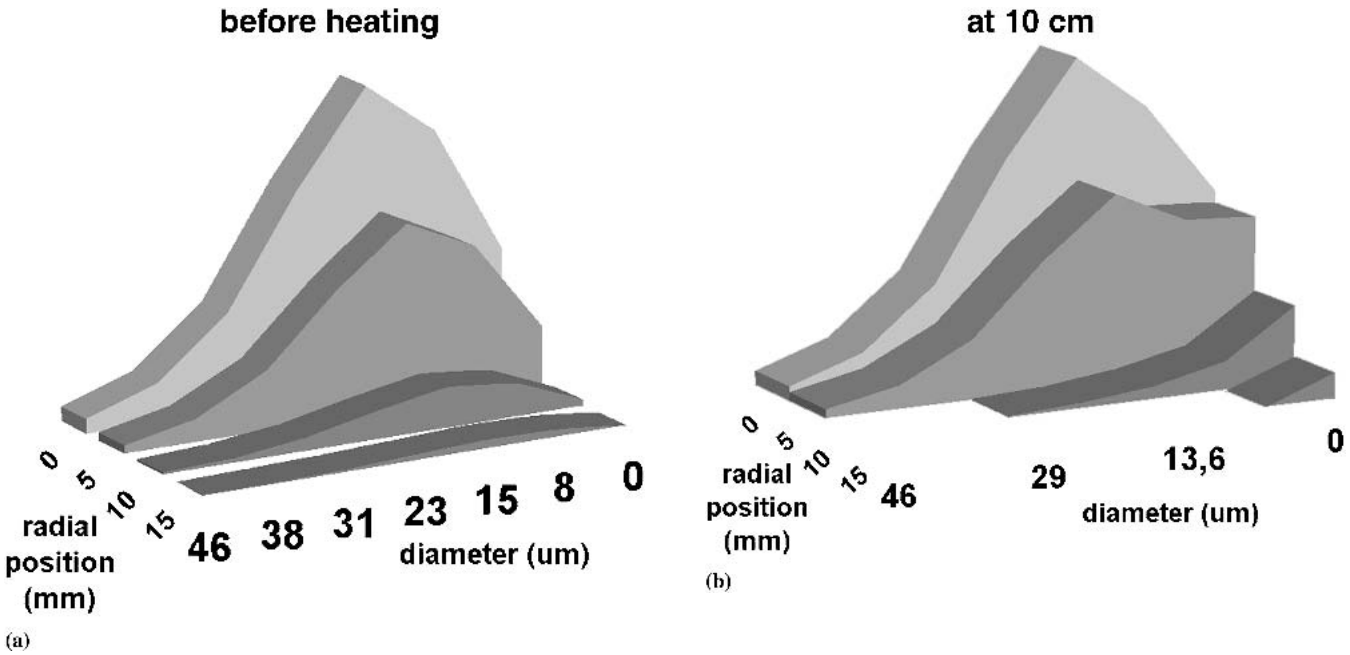

Fig. 7 **(a)** Predicted droplet diameter distribution vs radical position from the centerline of the flame-spray jet system before drying. Gun air pressure: 2 bars. **(b)** Droplet diameter distribution vs radial position from the centerline of the flame-spray jet system at 10 cm from the pneumatic gun exit. Gun air pressure: 2 bars

lost by vaporization. The droplets were assumed to have a uniform temperature. The equations were solved in a Lagrangian frame of reference moving with particles. The thermodynamic and transport properties of the air and flame mixture were determined using mixing laws from the properties of pure gases and composition of the gas system.[3] The model projected the trajectories of the droplets, their vaporization rate, and size evolution. The zirconia content of the droplets at impact was established from the droplet vaporization rate and initial solid content.

3.3.1 Droplet Trajectories. Figure 5 shows the predicted trajectories of the droplets with respect to a coordinate system aligned with the axis of the droplet spray jet after the intersection point with the flame. As expected, the deflection of the droplets from the flame-spray jet axis diminished as their diameter decreased. Therefore, the majority of the sprayed droplets, which diameter ranged between 18 and 35 μm, were moderately deflected from the main axis.

3.3.2 In-flight Droplet Evaporation and Solid Concentration in the Droplets at Impact. Most of the sprayed droplets followed a trajectory close to the centerline of the flame-spray system where the temperature was lower than in the fringes. According to the numerical simulations, the vaporization of droplets varied according to their trajectory as shown in Fig. 6. The droplets that traveled in the center of the spray jet maintained a high water content at impact (Fig. 7) if their original diameter was higher than 20 μm and initial solid concentration lower than 30%. On the other hand, the droplets that traveled in the fringes could be completely dried at impact and, therefore, behaved like solid particles when impinging on the substrate.

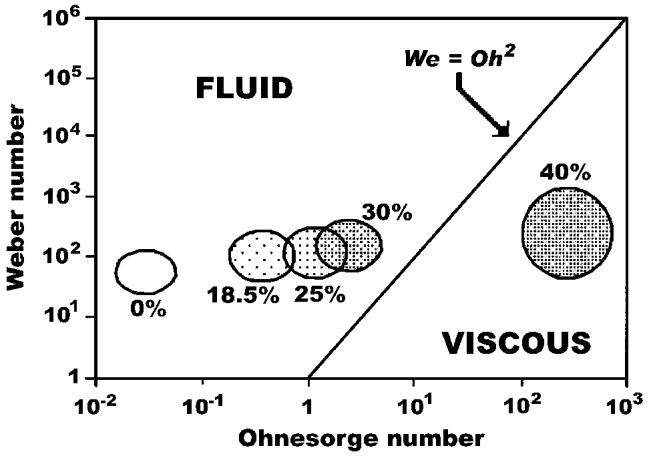

Fig. 8 Weber Number as a function of Ohnesorge number. The two regions characterize the impact of droplets onto smooth substrate depending on droplet conditions at impact after Schiaffino and Sonin.[19] The various circles correspond to the impact of droplets with different zirconia content. 0% corresponds to pure water droplets.

3.4 Droplet Impact on the Substrate

The prediction of droplet size, temperature, and velocity, combined with the hydrodynamic measurements realized in the present work allow estimation of the Reynolds (Re) and Weber (We) numbers of the droplets at impact. These dimensionless groups are characteristic of the impact and spreading process of the liquid on the substrate because (1) the Reynolds number quantifies the viscous dissipation of the inertia forces and (2) the

Table 1 Hydrodynamic Properties (Density ρ, Viscosity μ, Surface Tension σ, and Contact Angle θ) of Zirconia Sols With Various Solid Content

Solid Concentration, wt.%	ρ, kg/m^3	μ, mPas	σ, mN/m	θ, °
0 (pure water)	1000	1.0	72	0
18.5	1181	2.3	60.5	25.2
25.5	1268	20	55.2	34.5
30	1330	36	52.7	41.3
40	1496	2180	26.5	62.8

Table 2 Spreading Mechanisms of Droplets on a Substrate in Zones I and IV of the Schiaffino-Sonin Graph Shown in Fig. 8

Zone	Spreading Velocity	Spreading Time
I	V	D/V
IV	$\rho \cdot V^2 \cdot D/\mu$	$\mu/\rho \cdot V^2$

Table 3 (a) Predicted and (b) Experimental Values of Splat Maximum Diameter for Different Zirconia Concentration in Sol Droplets and Air Pressure of the Aerographic Gun

(a) Sol/Gun Pressure	2 bars	4 bars
5 wt.%	27 μm	42 μm
18.5 wt.%	30 μm	57 μm
(b) Sol/Gun Pressure	**2 bars**	**4 bars**
5 wt.%	35 μm	35 μm
18.5 wt.%	35 μm	25 μm

Weber number, the conversion of the kinetic energy into surface energy.

They are defined as:

$$\mathrm{Re} = \frac{\rho \cdot V \cdot D}{\mu} \quad \text{(Eq 2)}$$

$$\mathrm{We} = \frac{\rho \cdot V^2 \cdot D}{\sigma} \quad \text{(Eq 3)}$$

where D is the droplet diameter; V is the droplet velocity (m/s); ρ and μ is the density (kg/m^3) and the viscosity (Pa.s) of the liquid, and σ the surface tension (N/m).

Another dimensionless group, the Ohnesorge number that represents the resistance to spreading, characterizes the impact of a liquid droplet when no solidification constraint interferes with the flattening process. This dimensionless number is expressed as

$$\mathrm{Oh} = \frac{\mu}{\sqrt{\rho \cdot \sigma \cdot D}} = \frac{\sqrt{\mathrm{We}}}{\mathrm{Re}} \quad \text{(Eq 4)}$$

The plot of Weber number against Ohnesorge number, known as the Schiaffino-Sonin graph, may be divided in 4 zones

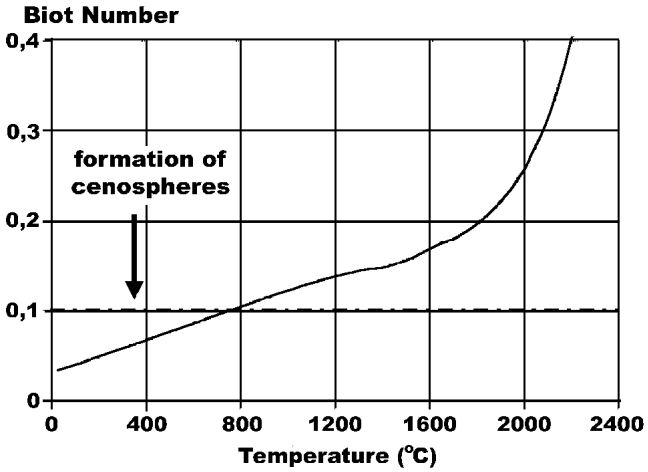

Fig. 9 Predicted effect of temperature on Biot number for water droplets in the flame-spray jet[3]

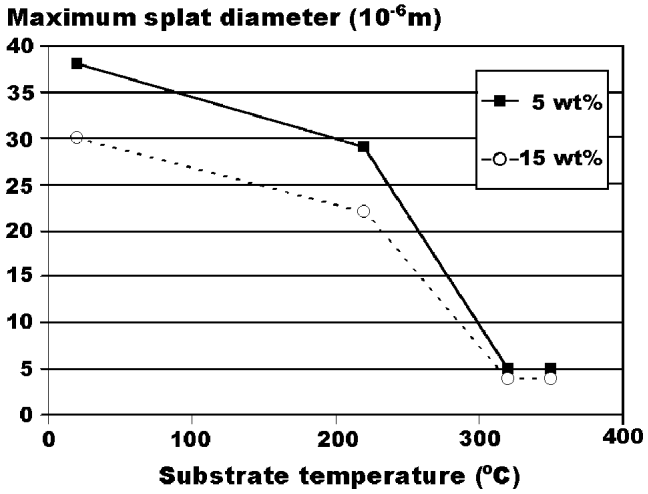

Fig. 10 Maximum splat diameter vs temperature for 5 and 15 wt.% sol concentrations. Aerographic gun air pressure: 4 bars

Table 4 Influence of Solid Concentration on the Morphology of the "Objects" Collected on the Substrate After Droplet Impact (X, Presence; XX, Majority)

Type of Objects/Solid Concentration	<15%	15-25%	25-40%
Splats	XX	X	X
Semi-Dry Cenospheres	X	XX	X
Dry Spheres and Cenospheres	X	X	XX

(see Ref. 19). The conditions of droplet impact, in this study, correspond to zones I and IV according to the zirconia solid concentration in droplets as represented in Fig. 8. These two zones are characteristic of "fluid flattening" and "viscous flattening." In that graph, the curve defined by We = Oh^2 corresponds to Re = 1. Reynolds numbers close to 1 (see Table 1) are typical of the impact of solid particles when the droplets are fully dried during

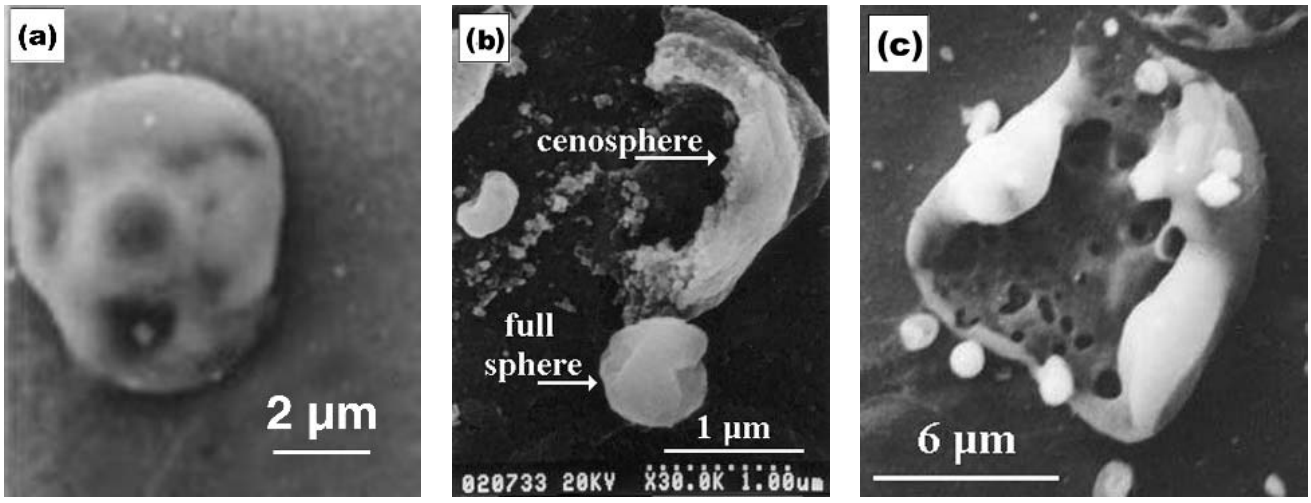

Fig. 11 SEM view of objects collecting on the substrate: **(a)** semi-dry flattening; substrate temperature: 25 ºC, **(b)** dry full sphere and dry cenosphere; substrate temperature: 220 ºC. **(c)** wet cenospheres; substrate temperature: 220 ºC

their residence in the flame. Higher values of Re are characteristic of wet or semi-wet state at impact. In that case, the liquid may spread onto the surface and form a lamella. The spreading velocity and time are depicted in Table 2.

The flattening rate ξ, defined as the ratio of the diameter of the lamella ($D_{lamella}$) to that of the original droplet ($D_{droplet}$), may be estimated from the equations proposed by Madejski[20] and Bennett et al. (cited in 13) for the "fluid" zone.

$$\text{Madejski equation: } = \frac{3\xi^2}{We} + \frac{1}{Re} \cdot \left(\frac{\xi}{1.2941} \right)^5 = 1 \qquad \text{(Eq 5)}$$

$$\text{Bennett equation: } = \frac{3[(1-\cos\theta)\xi^2 - 4]}{We} + \frac{1}{Re} \cdot \left(\frac{\xi}{1.2941} \right)^5 = 1 \qquad \text{(Eq 6)}$$

for Re and We > 100. θ is the contact angle of the liquid with the substrate. $\xi = D_{lamella}/D_{droplet}$.

However, other phenomena at impact make the estimation of lamella size and morphology tricky. Though Jones (cited in Ref. 21) assumed that the impinging droplets do not suffer physical changes during the spreading process, the contrary occurs in many cases[21] and the drying kinetics in suspension droplets may occur simultaneously with spreading. Nevertheless, Poirier[3] calculated that the drying time (assuming perfect thermal transfer between substrate and droplet) was about three times larger than spreading times in aqueous suspension droplets 30 μm in diameter and impacting with a velocity of 50-80 m/s on a substrate at 100 °C. This calculation showed that the Madejski and Bennett equations could be used with these impact conditions. Some authors[22,23] also considered the possibility that large fluid droplets may break up or explode if impact velocity or substrate temperature is too high. For example, Mundo et al.[22] considered that such splashing phenomenon occurs when the Sommerfeld number $K = \sqrt{We} \cdot \sqrt{Re}$ is higher than a critical value equal to 57.7 for pure water droplets. The roughness and surface chemistry of the substrate may also interfere

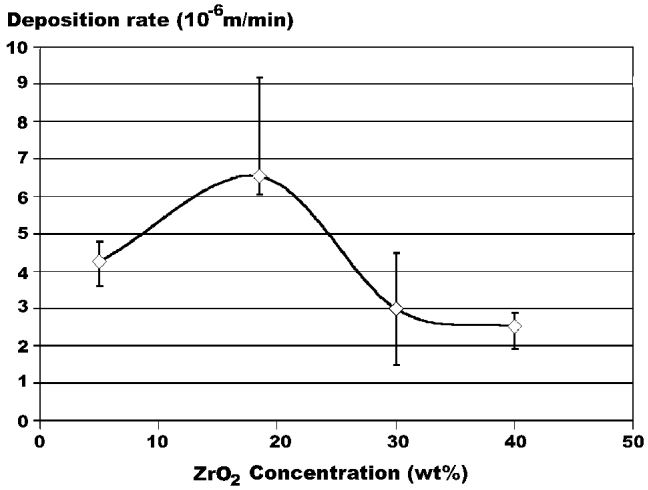

Fig. 12 Deposition rate vs sol concentration. Dots correspond to average value from 5 tests, bars correspond to minimum and maximum measured values.

with liquid spreading. In addition, Senda et al.[23] have observed that boiling of the liquid on the substrate can also cause breakup of the droplet instead of flattening and drying. Fukai et al.[10] established that the spreading diameter decreases with the substrate temperature up to the Leidenfrost point. This point corresponds to a minimum heat transfer rate between a sessile drop and a hot substrate and is also defined as the break up temperature of such drop. It is equal to about 290 °C for water. Above this point, Bernardin and Mudawar[24] showed that the impact velocity controls the final splat diameter and mostly results in boiling break up. Taking into account the mentioned criteria allows prediction of the final shape and diameter of the impinging droplets depending on their solid concentration. The latter was determined by modeling the droplet behavior in flight.

The splat diameter was predicted taking into account the former results and discarding the droplet diameters that would

result in splashing at impact. The predicted maximum splat diameters are presented in Table 3. The experimental observations by optical microscopy resulted in similar values for the maximum splat diameters. It is to note that the totally dried droplets did not adhere easily on the substrate and were more difficult to observe.

The SEM observation showed that few droplets splashed at impact as shown by the calculations.[3] However, not all the droplets flattened or behaved as dry particles. In some cases, some hollow crusts were formed due to poor water diffusion in the dried droplets. This phenomenon can be characterized by the Biot number (Bi) that represents the gas thermal resistance to the internal resistance of the droplet (Fig. 9):

$$\mathrm{Bi} = \frac{k_{\mathrm{hot\_gas}}}{k_{\mathrm{liquid}}} \qquad \text{(Eq 7)}$$

where $k_{\mathrm{hot\_gas\ is}}$ the thermal conductivity of the gas outside the boundary layer surrounding the droplet and k_{liquid} is the thermal conductivity of the liquid droplet.

When Bi > 0.1, the thermal diffusion was too high in com-

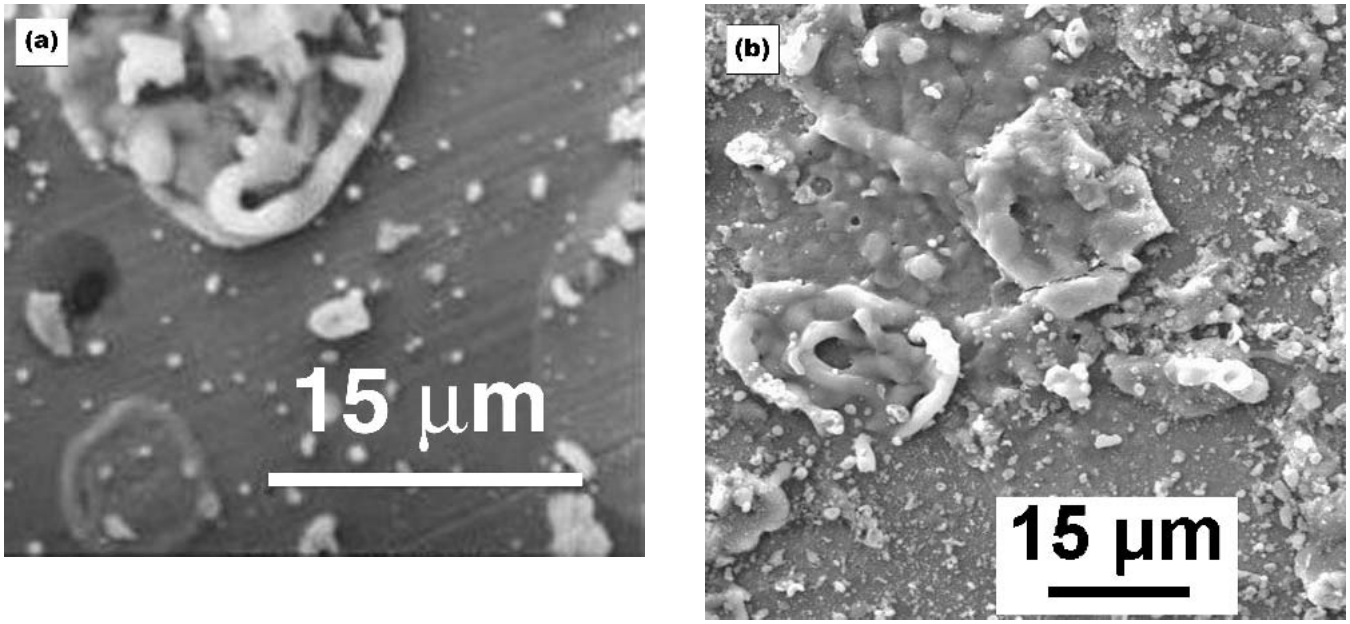

Fig. 13 Morphology of **(a)** flattened objects and **(b)** resulting coating for a 18.5 wt.% sol and an aerographic gun air pressure of 2 bars. No preheating. Depostion time: 40s

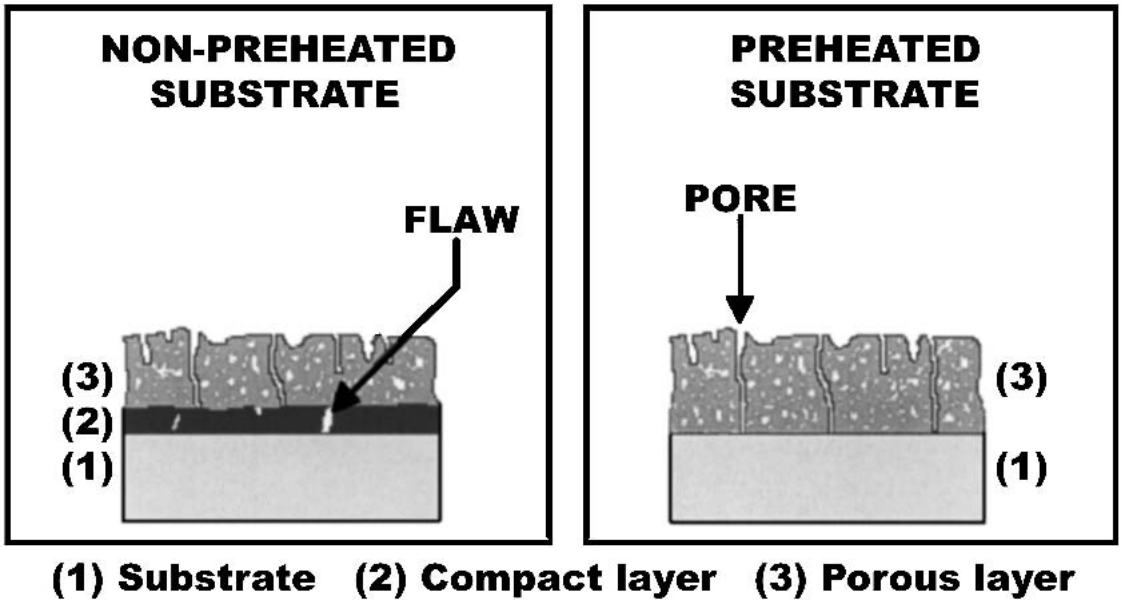

Fig. 14 Growing mechanism of coating for low-concentration sols

parison with water diffusion, and the crust which developed at the surface of the suspension droplet exploded in flight. Thus, "cenospheres" (hollow spheres) were formed and exhibited a dry or semi-dry aspect (Fig. 9). This behavior occurred especially when the fluid temperature was above 800 °C. This was the case at the periphery of the flame-spray jet. However, the droplets, which traveled in the peripheral region of the jet, were a minority. This cenosphere effect explains the difference between predictions and experimental results (Table 3), particularly in the case of the 18.5 wt.% zirconia sol sprayed with an air pressure of 4 bars.

The original solid concentration in the sol droplets also controlled the aspects of the flattened droplets, as depicted in Table 4. Additionally, a decrease in splat diameter was observed when the substrate temperature increased (Fig. 10) above the Leidenfrost point as shown by Fukai[10] and Bernardin.[6] As a consequence of boiling at the interface between substrate and droplets, an open porosity was observed by SEM (Fig. 2b) and atomic force microscopy.[3] The particular shape of the borders of the semi-dry cenospheres (Fig. 11c) suggested a plastic deformation. The observation of the area in contact with the hot substrate gave evidence of a boiling effect from the droplet-substrate interface. This confirmed the presence of residual water at impact. The hollow aspect also suggested that the center of the impinging droplet was richer in liquid than the pasty crust. This observation is quite consistent with the Biot number predictions, even in the centerline of the jet (400 °C). When Bi is higher than 0.07-0.1, a slow water diffusion took place in the in-flight droplet through the crust and yielded a predominance of cenospheres above splats, especially for the large droplets.

3.5 Coating Formation

The knowledge of the final shape of the impinging droplets is essential to understand the formation of the coating. The deposition rate (Fig. 12) of the coating increased up to 6 μm/min as the sol concentration increased up to about 20%. Above this value, the droplets had poor residual moisture and were less ad-

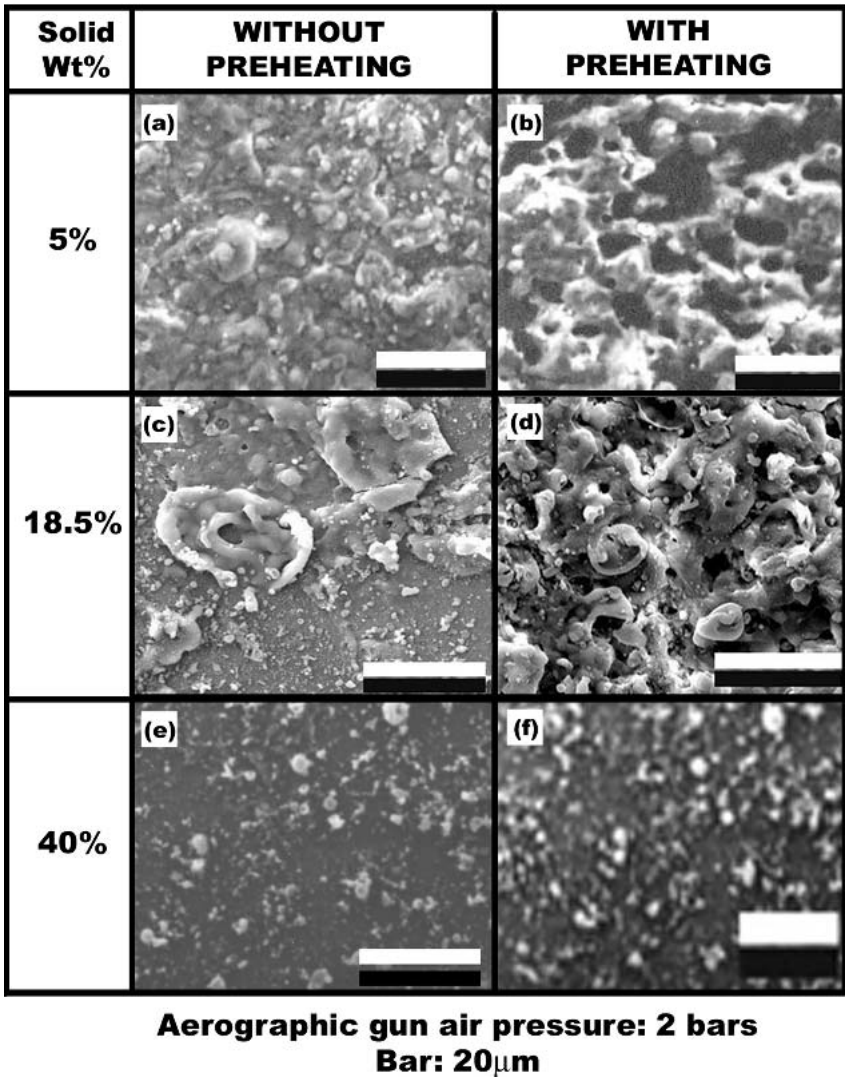

Fig. 15 Evolution of coating morphology vs droplet solid concentration when the substrate is preheated at 250 ºC or kept at ambient temperature (aerographic gun air pressure: 2 bars). Bar 20 μm

herent to the substrate. Good agreement was observed between the morphology of the coating and single droplets collected on the substrate surface as shown in Fig. 13(a) and (b). Substrate preheating was found to affect partly the coating aspect as the substrate temperature determines the boiling effect and efficiency of the thermal transfer between the wet droplets and the substrate. When the substrate was preheated to an optimum temperature of about 250-300 °C, the coating made with a low-concentrated sol was highly porous. With no preheating, the first layers of coating were dense and subjected to slight flawing, until the substrate temperature reached 250-300 °C. Then, the layers became porous and flawless resulting in a two-layered coating (Fig. 14). Such a phenomenon was due to the elimination of residual water of in-flight partially dried droplets: a "less warm" substrate (<250 °C) did not allow the complete elimination of the residual water of droplets since splats were formed and stuck one to another. When the temperature increased, this water was expelled and caused cracks in the dense coating. When the droplets impinged on a hotter surface (>250 °C), the elimination of residual water occurred immediately at impact and brought about porosity. The less concentrated the sol was, the larger were the pores. When sol concentration is higher than 20%, the preheating did not affect the coating morphology (Fig. 15).

4. Conclusion

In spite of the complexity of the geometry of the suspension spray-flame mixture and the diversity of the thermal histories of the droplets, the observation of the droplets after impact on metallic substrates showed that the predictions of a 2D model projecting the heating, vaporization and acceleration of the droplets are quite consistent with the experimental observations. Thus, the proposed method has proved to be a useful tool to simulate the complex mechanisms of the injection and drying of droplets in a flame and predict their behavior at impact. Such predictions can contribute to a better understanding of the mechanisms governing the formation of AFS coatings that are closely related to splat morphology. It can also help to take advantage of the versatility of the process for controlling the coating microstructure.

References

1. J. Karthikeyan, C. Berndt, S. Reddy, J.-Y. Wang, A. King, and H. Herman: "Nanomaterial Deposits Formed by DC Plasma Spraying of Liquid Feedstocks," *J. Am. Ceram. Soc.* 1998, *81*(1), pp. 121-28.
2. A.R. Di Giampaolo, H. Reveron, H. Ruiz, T. Poirier, J. Lira, and H. Vesteghem: "Zirconia Coatings on Stainless Steel by Aerosol Thermal Spraying," *A.T.M,* 1998, *1*(1), pp. 90-100.
3. T. Poirier: "Zirconia Coatings Manufactured by Aerosol Flame Spraying," Ph.D. Thesis, Université de Limoges, France, Nb: 49-2000 (in French).
4. H. Vesteghem, A. Lecomte, and A. Dauger: "Film Formation and Sintering of Colloidal Monoclinic Zirconia," *J. Non. Cryst. Solids,* 1992, *147,148,* pp. 503-507.
5. H. Reveron: "Synthesis of Cerium-Partially Stabilized Zirconia," Ph.D. Thesis, Université de Limoges, France, Nb: 51-2000 (in French).
6. J. Bernardin, C. Stebbins, and I. Mudawar: "Mapping of Impact and Heat Transfer Regimes of Water Drops Impinging on a Polished Surface," *Int. J. Heat Mass Transfer,* 1997, *40*(2), pp. 247-67.
7. M. Ciofalo, I. Di Piazza, and V. Brucato: "Investigation of the Cooling of Hot Walls by Liquid Water Sprays," *Int. J. Heat Mass Transfer,* 1999, *42,* pp. 1157-75.
8. Z. Liu and R. Reitz: "Modeling Fuel Spray Impingement and Heat Transfer Between Spray and Wall in Direct Injection Diesel Engines," *Numerical Heat Transfer,* Part A, 1995, *28,* pp. 515-29.
9. W.J. Yang: "Natural Convection in Evaporating Droplets" in *Handbook of Heat and Mass Transfer, Vol. 1, Heat Transfer Operations,* N.P Cheremesinoff, ed., Golf Publishing Co., Houston, 1986, pp. 211-28.
10. J. Fukai, Y. Shiiba, and O. Miyatake: "Theoretical Study of Droplet Impingement on a Solid Surface Below the Leidenfrost Temperature," *Int. J. Heat Mass Transfer,* 1997, *40*(10), pp. 2490-92.
11. V. Sobolev: "Formation of Splat Morphology During Thermal Spraying," *Materials Letters,* 1998, *36,* pp. 123-127
12. M. Pasandideh-Fard, J. Mostaghimi, and S. Chandra: "3D Model of Droplet Impact and Solidification: Impact on a Solidified Splat" in *Proceedings of the 14th International Symposium on Plasma Chemistry,* M. Hrabovský, M. Konrád, and V. Kopecký, ed., Institute of Plasma Physics, Prague, 1999, pp. 2081-87.
13. A.C. Léger: "Experimental Study of Splat Formation and Residual Stresses in Plasma-Sprayed Coatings," Ph.D. Thesis, Université de Limoges, France, Nb: 4-1997 (in French).
14. J.J Bikerman, *Physical Surfaces,* Academic Press, London, United Kingdom, 1970, pp. 16-19.
15. K. Masters: *Spray Drying,* 2nd ed., J. Wiley, New York, 1976, pp. 206-84.
16. H. Ruiz: Technical Report, Surface and Interface Engineering Group, Universidad Simon Bolivar, Caracas, Venezuela, 1995.
17. P. Arques: *Inflammation, Combustion, Pollution,* Masson, Paris, France, 1992, pp. 6-11.
18. A. Vardelle: "Modeling of the Heat, Mass and Momentum Transfers Between DC Plasma Jets and Particles," D.Sc. State Thesis, University of Limoges, France, Nb 27-87, 1987.
19. S. Schiaffino and A. Sonin: "Molten Droplet Deposition and Solidification at Low Weber Numbers," *Phys. Fluids,* 1997, *9,* pp. 3172-87.
20. J. Madejski: "Solidification of Droplets on a Cold Surface," *Int. J. Heat Mass Transfer,* 1976, *19,* pp. 1009-1013.
21. L. Bianchi: "DC and RF Plasma Spraying of Ceramic Coatings: Mechanisms of Formation of the First Layer and Relationship With the Mechanical Properties of the Coating," Ph.D. Thesis, Université de Limoges, Nb: 41-1995 (in French).
22. C. Mundo, M. Sommerfeld, and C. Tropea: "Droplet-Wall Collisions: Experimental Studies of the Deformation and Break-up Process," *Int. J. Multiphase Flow,* 1995, *21*(2), pp. 151-73.
23. J.Senda, M.Kobayashi, S.Iwashita, and H. Fujimoto: "Modeling of Diesel Spray Impinging on Flat Wall," *JSME Int. J., Series B.,* 1996, *39*(4), pp. 859-86.
24. J.Bernardin and I.Mudawar: "Film Boiling Heat Transfer of Droplet Streams and Sprays," *Int. J. Heat Mass Transfer,* 1997, *40*(11), pp. 2579-93.